Title

Multichromatic Near-Infrared Imaging to Assess Interstitial Lymphatic and Venous Uptake *In Vivo*

Authors

Fabrice C. Bernard[1], Jarred Kaiser[2], Sarvgna K. Raval[2], Zhanna V. Nepiyushchikh[3], Thanh N. Doan[2], Nick J. Willett[1,2,4,5], J. Brandon Dixon[1,3,5]

[1]Wallace H. Coulter Department of Biomedical Engineering, Georgia Institute of Technology and Emory University, Atlanta, GA

[2]Department of Orthopaedics, Emory University, Atlanta, GA

[3]George W. Woodruff School of Mechanical Engineering, Georgia Institute of Technology, Atlanta, GA

[4]Department of Orthopaedics, Atlanta Veteran's Affairs Medical Center, Atlanta, GA

[5]Parker H. Petit Institute for Bioengineering and Bioscience, Georgia Institute of Technology, Atlanta, GA

* Correspondence:
J. Brandon Dixon
Georgia Institute of Technology
315 Ferst Drive
Room 2312
Atlanta, GA 30332
Telephone: 404-385-3915
Email: dixon@gatech.edu

* Correspondence:
Nick J. Willett
Atlanta Veteran Affairs Medical Center
1670 Clairmont Rd
Room 5A-115
Decatur, GA 30033

Telephone: 404-321-6111, ext. 3248
Email: nick.willett@emory.edu

Abstract

Significance: Changes in interstitial fluid clearance are implicated in many diseases. Using NIR imaging with properly sized tracers could enhance our understanding of how venous and lymphatic drainage are involved in disease progression or enhance drug delivery strategies.

Aim: We investigated multichromatic NIR imaging with multiple tracers to assess *in vivo* microvascular clearance kinetics and pathways in different tissue spaces.

Approach: We used a chemically inert IR Dye 800CW (free dye) to target venous capillaries and a purified conjugate of IR Dye 680RD with a 40 kDa PEG (PEG) to target lymphatic capillaries *in vivo*. Optical imaging settings were validated and tuned *in vitro* using tissue phantoms. We investigated multichromatic NIR imaging's utility in two *in vivo* tissue beds – the mouse tail and rat knee joint. We then tested the ability of the approach to detect interstitial fluid perturbations due to exercise.

Results: In an *in vitro* simulated tissue environment, free dye and PEG mixture allowed for simultaneous detection without interference. Co-injected NIR tracers cleared from the interstitial space via distinct routes allowed assessment lymphatic and venous uptake in the mouse tail. We determined that exercise after injection transiently increased lymphatic drainage as measured by lower normalized intensity immediately after exercise, while exercise pre-injection exhibited a transient delay in clearance from the joint

Conclusions: NIR imaging enables of simultaneous imaging of lymphatic and venous-mediated fluid clearance with great sensitivity and can be used to measure transient changes in clearance rates and pathways.

Key Words

Tissue Optics, NIR Imaging, Venous, Lymphatic, Clearance

Introduction

The circulatory system maintains tissue homeostasis through the continuous delivery of nutrients and oxygen to the tissue space and the removal of proteins and waste products. Crucial to this process is the removal of interstitial fluid, proteins, and lipids by the lymphatic vasculature; this fluid then returns to the circulation through absorption at the lymph nodes and delivery to the central venous system through the lymphatic ducts. Recent developments in optical imaging have provided new capabilities to quantify lymphatic function *in vivo*.

Generally, there are two routes of fluid clearance from tissues: 1) venous uptake and 2) lymphatic uptake. Venous return in tissue beds is passive, size-dependent, and varies based on capillary physiology[1,2]. In contrast, lymphatic capillaries originate from the tissues and have flap-like openings, which non-discriminately allow molecules of all sizes to enter. The extrinsic motion of the surrounding tissue combined with the intrinsic contractility of downstream lymphatics, create transient pressure gradients that allow fluid and macromolecules to enter the vessel and be transported downstream. Impaired interstitial fluid clearance has been implicated in various diseases, including lymphedema[3], cancer[4], and arthritis[5]. Techniques to measure clearance kinetics from interstitial spaces are critical to evaluating disease state and different tissues' ability to drain molecules from the interstitial spaces. These measurements have been assessed classically via radiolabeled agents, which carry potential toxicity and require additional safety measures [6–8]. However, the advent of near-infrared (NIR) fluorescent imaging allows for cost-effective, high resolution, clinical and preclinical imaging in a variety of applications[9–11].

NIR-based technologies have advanced considerably in the last decade—both in terms of imaging components as well as tracers and fluorophore-based probes—which have allowed for significant new *in vivo* capabilities. The NIR imaging window includes the visible and infrared light spectrum from 650-1300 nm, which due to longer wavelengths, penetrates tissues deeper than higher energy light[12–14]. Contrast agents like indocyanine green (ICG), polyethylene glycol (PEG) conjugated with NIR dyes, or NIR quantum dots have been used to visualize lymphatics and blood vessels *in vivo* [15–19]. Preclinical NIR imaging has also previously enabled the measurement of tracers' differential uptake as a function of size from different tissue beds[17,20]. Multichromatic NIR imaging (e.g., imaging with multiple NIR fluorescent probes) empowers mapping of the drainage zones of lymph nodes in rodents[19,21,22]. However, this has not yet been

92 widely extended to differentiate between venous uptake and lymphatic uptake simultaneously in
93 the same tissue bed.
94 We have previously shown the size-dependent uptake of 2 and 40 kDa NIR PEG into the
95 venous and lymphatic circulation, respectively, after injection into the rat knee joint[23]. In that
96 study, we demonstrated that the intra-articular injection of endothelin-1 (ET-1), a vasoactive
97 compound in lymphatics and veins, transiently reduced the outflow of both PEG tracers from the
98 joint in a dose-dependent manner. Due to these experiments' monochromatic nature, we were
99 unable to assess lymphatic and venous drainage simultaneously. The inability to differentiate
100 clearance mechanisms and function between the venous and lymphatic systems is a critical
101 technological gap that has broad implications for many different tissues and disease states.
102 Coupling *in vivo* delivery with multichromatic NIR imaging could allow for the advancement of
103 the understanding of how the venous and lymphatic drainage may change in the context of
104 diseases or physical interventions. The objective of this manuscript was to develop a novel
105 technological approach that couples NIR imaging with the size-dependent clearance of tracers *in*
106 *vivo*. We hypothesized that a multichromatic imaging approach for differentially imaging the
107 lymphatic and venous systems would show the technique's utility in both the mouse tail, where
108 the superficial vessels can be clearly visualized, and in the rat knee joint, where uptake occurs
109 slowly and in deeper tissue structures. Additionally, we perturbed the joint microenvironment by
110 exercising the rats on a treadmill and detected changes in venous and lymphatic clearance within
111 the knee joint.
112
113 **Methods**
114 **Tracers for *in vivo* injection**
115 IR Dye 800CW carboxylate (free dye) (LI-COR Biosciences) was purchased as a dry
116 lyophilized powder. 20 nanomoles were resuspended in 100 µl of sterile saline to make a 20 mM
117 stock solution and used within a few days of resuspension. For tail injections, 2.5 µl of the stock
118 solution was used. For tissue phantom studies and knee injections, the stock solution was diluted
119 to 0.4 mM in sterile saline.
120 40 kDa methoxy polyethylene glycol (PEG) amine (JenKem Technology) was purchased
121 as a dry lyophilized powder for PEG tracer synthesis. To conjugate 40 kDa PEG amine to IR
122 Dye 680RD, 16 mg of PEG amine was reacted with 30 µl of 10 mg/ml IR Dye 680RD NHS ester

123 (diluted in dimethyl sulfoxide (DMSO)) in a total of 1 ml of Dulbecco's Phosphate-Buffered
124 Saline (DPBS) overnight. Unreacted IR Dye, salts, and DMSO were removed via centrifugal
125 filtration using deionized water and a 10 kDa molecular weight cutoff centrifugal filters (Amicon
126 Ultra). After centrifugation, the purified tracers were separated into 10 equal volumes of 100 µl
127 and aliquoted to 1.6 mg of tracer per aliquot, lyophilized, and kept frozen at -20°C for long term
128 storage. For tail injections, aliquots were resuspended in 100 µl of sterile saline, and 2.5 µl of
129 P40D680 was injected intradermally. For tissue phantom studies and knee clearance studies,
130 aliquots were diluted to 1 mg/ml.
131
132 **Optical properties of tracers**
133 To quantify each tracer's absorbance in the visible and NIR range, 0.4 mM, and 1 mg/mL
134 of the free dye and 1mg/mL of PEG were loaded into a standard UV/vis spectrophotometer
135 (Ultraspec 2100, Biochrom). The emission and excitation spectra of free dye and PEG were
136 assessed using a microplate reader with filter-based emission and detection capabilities (Synergy
137 H4, BioTek). For PEG and free dye, fixed emission filters of 720 and 840 nm were used while
138 sweeping the excitation source from 400 – 700 and 400 – 820 nm, respectively, to generate
139 excitation curves. Following the excitation sweeps, fixed excitation wavelengths of 660 and 760
140 were used to conduct an emission sweep from 680/780 – 900 nm for PEG and free dye.
141
142 **NIR imaging setup**
143 Multichromatic NIR imaging was carried out using a customized NIR setup [17,24]. Briefly,
144 the system consists of a cooled EMCCD camera (Evolve eXcelon, Photometrics) attached to a
145 stereomicroscope with adjustable zoom (MVX10, Olympus), a shutter-controlled xenon arc light
146 source (Lambda LS, Sutter Instrument Company), and a manual filter wheel equipped with
147 standard Cy5.5 and ICG-B filter cubes (Chroma Technology). The electronic shutter was left
148 open during continuous imaging sessions, and images were acquired using MicroManager
149 software [25].
150
151 **Dye and tracer characterization and tissue phantom studies**
152 Polydimethylsiloxane (PDMS) tissue phantoms, measuring 2 and 4 mm in thickness,
153 were created using a previously described protocol[15]. By weight, 88.10% silicone elastomer base

154 (Sylgard 184, Dow Corning) was mixed with 8.81% curing agent (Sylgard 184, Dow Corning),
155 1.76% Aluminum Oxide (Sigma Aldrich), and 1.32% cosmetic powder (Max Factor Crème Puff
156 Deep Beige 42). PDMS phantoms were poured into plastic molds and left to cure in the oven at
157 60°C overnight.

158 To obtain reference measurements for our NIR imagine setup, stock PEG and free dye
159 were diluted serially in two-fold dilutions in PBS. In separate 1.5 ml centrifuge tubes, free dye
160 and PEG were diluted using PBS to 0.4 mM and 1 mg/ml. The tissue phantoms were used to
161 demonstrate the effect of tissue depth on tracer intensity with the previous serially diluted
162 samples. To simulate increasing tissue depth each centrifuge tube was imaged with no tissue
163 phantom or with a 2- or 4-mm tissue phantom. To quantify the sensitivity to each tracer in the
164 presence of the other NIR tracer, each tracer was diluted using the stock solution of the other
165 tracer. The 2 mm tissue phantom was used to mimic the typical depth of the superficial
166 collecting lymphatics in rodents. All images were taken with an exposure time of 50 and 5
167 milliseconds, respectively, for free dye and PEG.

168

169 **Tail injections to visualize and quantify routes of tracer clearance**

170 To visualize the tail lymphatics and blood vessels, 20 µl of 1% (w/v) Evans blue solution
171 was injected into the tip of the tail of an anesthetized mouse. Evans blue binds to interstitial
172 proteins and is mainly taken up by lymphatics when injected intradermally. Post-euthanasia the
173 skin was removed at the base of the tail to reveal the underlying vasculature. Images of the
174 vasculature were taken using a standard color camera to provide a comparison with NIR images.
175 For NIR imaging through the skin, isoflurane was used to anesthetize C57Bl/6J mice, and the
176 animal was placed in a recumbent position (on its side). A mixture containing 2.5 µl of the free
177 dye and 2.5 µl of PEG was mixed and loaded into 1 mL insulin syringes (Becton Dickinson) and
178 injected intradermally into the tip of the tail. After injection, standard tape was gently applied to
179 the base and the end of the tail to minimize drift from motion artifact during imaging. Free dye
180 and PEG signals were imaged in 2-minute increments by manually changing the filter wheel to
181 select the appropriate filter set every 1200 frames (Figure 1a). The free dye and PEG signal were
182 evaluated at 50 and 20 milliseconds, respectively, and images were captured at ten frames per
183 second.

Animal care and experiments were conducted under the institutional guidelines of the Georgia Institute of Technology. Experimental procedures were approved by the Georgia Institute of Technology Institutional Animal Care and Use Committee (IACUC).

Intra-articular injections for clearance

Male Lewis rats weighing 350-400 grams were trained to run on the treadmill over two weeks. On day one, the rats were acclimated to the treadmill for 30 minutes without running. On day two, the treadmill was speed was set to 5 m/min for 5 minutes and 0 m/min for 25 minutes. Each day the time spent running was increased by 5 minutes a day until the rats could run for 30 minutes on consecutive days after two weeks. Rats that failed to walk the targeted duration twice over the training course were excluded from the study. All other rats were then randomly selected for the experimental procedure to either run or serve as controls for the study duration. Three sets of experiments were conducted with these two rat groups: 1) rats that did not run on the treadmill and were co-injected bilaterally with NIR tracers (No Running), 2) rats that were run on the treadmill for 30 minutes before injection (Pre-Injection Running), 3) rats that were run on the treadmill for 30 minutes immediately after injection (Post-Injection Running).

The day before the experiment, all rats were anesthetized, the hair was removed from the knees and lower abdomen, and background images of the knees were taken. Before imaging, each rat was induced via 5% isoflurane on the day of the experiment, which was maintained at 2% after induction. Tracers were injected in both knees and imaged at set time intervals (approximately 0, 1, 2, 3, 5, 7 12, & 24 hours) over the course of 24 hours.

Animal care and experiments were conducted per the institutional guidelines of the Atlanta Veteran Affairs Medical Center (VAMC). Experimental procedures were approved by the Atlanta VAMC IACUC.

Image processing and analysis

Images captured using our custom NIR imaging system were saved as 16-bit depth 512 x 512-pixel TIF file format. For both tissue phantom experiments and *in vivo* knee joint clearance experiments, the tracer's intensity in the image was quantified using a custom MATLAB (MathWorks) script. The ROI for each image was quantified by averaging the 5% highest pixel intensities. This ROI visually corresponded with the size and position of the knee space shown in

Figure 1b. Data points were fitted to a monoexponential function $f(t) = y0 + Ae^{-kt}$, where y0 is the offset, t is the time in hours, A is the normalized peak fluorescence at the maximum intensity, and k is the time constant. τ (tau) was determined as the inverse of the time constant. To compare each intervention's short-term effects, we calculated the mean change in ROI intensity over the first hour and subtracted the mean value of internal control rats. To determine each intervention's overall effects, we calculated the time constant for each runner and normalized it to the non-runner group's mean.

For mouse tail injections of NIR dyes, the filter was changed manually every 2 minutes. To remove imaging artifacts from the manual changing of the filter, 60 seconds (600 frames) of each imaging window were cropped. Fiji software was used to crop, register, and quantify regions of interest (ROIs)[26]. An ROI was drawn on the blood and lymphatic vessels to monitor the signal of free dye and PEG over the experiment.

Data presentation and statistics

All clearance data are presented as mean ± SEM. A Brown-Forsythe test was used to quantify if variances were significantly different. A student's t-test with a Welch's correction was used to compare venous and lymphatic area under the curve and tau in control rats. A one-way ANOVA with Dunnett's multiple comparison test was used to calculate statistical significance for exercise studies.

Results

Optimization and characterization of NIR tracers using an *in vitro* tissue phantom

Absorbance spectra of free dye and PEG display an absorption maximum of 765 nm and 672 nm, respectively (Figure 2a). Emission and excitation spectra for these tracers also show each tracer's expected maxima referenced to the full-width half maximum of the filter sets on the imaging system (Figure 2b). To determine the limits of detection in our imaging system as a function of concentration and tissue depth, we used tissue phantoms. Individual tracers were imaged in 1.5 ml centrifuge tubes with and without 2- and 4-mm phantoms. Increasing the tissue phantom thickness decreased the fluorescent intensity, though even at 4 mm, the dyes could be detected at a concentration of 3% of the injection concentration (Figure 2c). At a thickness of 2mm, which is within the depth of most superficial lymphatics in rodents, this detection limit

246 was less than 1% of the injection site's intensity. Notably, mixing the tracers did not affect the
247 sensitivity to detect one dye when contained in the background of the other tracer (Figure 2d).
248
249 **NIR tracers of different size exit through spatially distinct clearance pathways**
250 The mouse tail's unique circulatory and lymphatic vasculature was visualized via
251 intradermal injection of Evans blue and skin removal. The lymphatics immediately cleared
252 Evans blue allowing clear visualization of the two lymphatic vessels running parallel to the tail
253 vein and artery (Figure 3a). To simultaneously quantify lymphatic and venous drainage, these
254 tracers were co-injected in the mouse tail. Images for each tracer were captured during two-
255 minute imaging windows (eight recordings per tracer). Figure 3b shows that the routes of
256 clearance of free dye in the blood circulation (red) and PEG dye in the lymphatics (blue) 10
257 minutes post-injection are spatially distinct and match the expected physiology where two
258 lymphatic vessels flank a blood vessel. The free dye was initially detected in the lymphatic
259 within the first imaging window (Supplementary Video 2) as the free dye is not expected to be
260 excluded by lymphatics. The free dye intensity increased between the first, third, and fifth
261 imaging windows and remains constant by the seventh (Figure 3d). However, PEG entered the
262 lymphatics after injection and did not appear in the bloodstream over this time interval,
263 demonstrating the lymphatic specificity of PEG (Supplementary Video 1). Also, the lymphatic
264 tracer exhibited strong transient peaks in the signal intensity due to intrinsic phasic lymphatic
265 contractions. In contrast, no such peaks were present in the tracer taken up into the blood
266 circulation.
267
268 **Co-injection to assess differential tracer clearance in the joint**
269 The effect of exercise on intra-articular clearance has not been extensively studied[27,28] ,
270 specifically in quantifying the change in venous and lymphatic drainage. Therefore, after
271 confirming size-dependent uptake from the tail, we used multichromatic imaging to assess intra-
272 articular drainage. Unlike intradermal injections, materials from the joint space clear much
273 slower [29–31]; therefore, venous and lymphatic clearance from this interstitial depot was expected
274 to occur over one day. Simultaneously injected tracer clearance PEG and free dye profiles
275 (Figure 4a) exhibited an initial increase followed by monoexponential clearance kinetics
276 consistent with previously reported figures[23]. Specifically, lymphatic tracers showed a more

substantial increase in intensity after the injection, whereas this increase was less pronounced for the venous tracer. By 12 hours post-injection, the intensity of the free dye was not detectable (Figure 4a). The normalized area under the curve (AUC) for free dye was calculated to be 3.59 ± 0.18 and 18.57± 1.33 for PEG ($p<0.0001$), demonstrating significant retention of the PEG in the joint space (Figure 4b). The time constant (Tau) for the clearance of free dye was calculated to be 4.28 ± 0.25 hrs, while the time constant for PEG was 7.11 ± 0.51 hrs ($p=0.0003$) (Figure 4c). A detectable amount of the PEG tracer remained in the joint space even after 24 hours (Figure 4a), likely due to some PEG tracer remaining trapped in the interstitium.

Multichromatic imaging for measuring patterns in joint clearance

To demonstrate the utility and sensitivity of multichromatic imaging to evaluate differential changes in clearance mechanisms for venous and lymphatic drainage, animals were exercised either pre- or post-injection. In rats that received no running intervention, clearance curves for both lymphatic and venous tracers had clearance profiles as expected. (Figure 5a). Qualitatively, from the initial injections, there did not appear to be differences in differences in the traces of animals that were designated runners and control animals. To quantitatively evaluate these differences, the normalized changes in fluorescence intensity were calculated (Fig 6a, c), as well as the time constant (Fig 6b, d).

For venous drainage, running pre-injection (0.26 ± 0.10) significantly increased ($p = 0.04$) the change in fluorescence intensity compared to running post-injection (-0.03 ± 0.06), however neither were significantly different from control (0.06 ± 0.06) (Figure 6a). Figure 6c shows the normalized tau (venous) for running post-injection was calculated to be (0.79 ± 0.13) which is significantly reduced ($p = 0.04$) the compared to pre-injection running (1.188 ± 0.12) (Figure 6c) however neither were significantly different than controls (1.16 ± 0.05).

When assessing lymphatic clearance, we observed a significant reduction ($p = 0.0003$ and $p = 0.01$) in the initial change in fluorescent intensity in running post-injection (-0.19 ± 0.05) compared to pre-injection (0.36 ± 0.1) and non-running controls (0.20 ± 0.1) (Figure 6b). however, we did not observe any significant change in tau for lymphatic tracers for the various conditions of running (Figure 6d). These data suggest the transient effect of running may be lost over the much longer timescale for which lymphatic clearance occurs.

Discussion

In this manuscript, we demonstrated the ability of multichromatic NIR imaging's ability to assess interstitial clearance mechanisms from multiple tissue beds. Clearance pathways and rates are essential in tissue homeostasis and dictate how biomolecules interact with their intended targets. Clearance to lymphatics or venous circulation has is understudied *in vivo*. Using tissue phantoms, we established the exposure time and tissue depth limitations required for *in vivo* imaging. We determined that sensitivity/cross talk between the dyes did not exist, confirming that the changes in signal intensity resulted from changes in concentration or position of our tracers within our ROIs. We then used the mouse tail, a tissue drainage bed with well-defined physiology, to show that we could target lymphatic and venous circulation and quantify function. Lastly, we demonstrated the capacity to quantitatively image routes of clearance from the joint space. We utilized an exercise-based intervention to confirm that the technique had the sensitivity to assess clearance changes.

Our study demonstrated the size dependence of interstitial molecules via venous and lymphatic pathways via simultaneous imaging. Proulx et al. showed that NIR tracers that clear through lymphatics have a delayed uptake into the systemic circulation compared to molecules that drain directly into the blood stream[18]. In our moues tail study, the free dye intensity in the blood ROI is initially low. That signal intensifies in the tail vein over time, likely due to a renal clearance not surpassing the intradermal depot clearance over this total imaging window[32]. Thus, this dye's intensity in the blood circulation continuously increases as the concentration delivered to the blood over time increases. The PEG tracer signal intensity traces exhibited the characteristic phasic contractions attributed to lymphatic pumping. Therefore, our mouse tail experiment validated our two tracers' size-based partitioning to distinct routes of clearance.

The joint space is a unique interstitial space comprised of synovial fluid—hyaluronic acid, lubricin, and filtered serum—that hydrates the joint tissues and buffers the outflow of materials from the joint space[33,34]. A solute that leaves the joint space must diffuse through the synovial fluid, then into the synovial membrane. The synovial membrane is a specialized tissue that retains the synovial fluid while also housing the venous and lymphatic fluid exchange machinery to clear solute from the joint[25,35]. Smaller materials can more easily diffuse through the synovial fluid matrix and thus exit the joint space faster[36]. Larger molecules can more easily entangle in the synovial fluid matrix and therefore have longer residence times within the joint

339 space[37]. Using multichromatic imaging with sized tracers enables quantifying venous and
340 lymphatic clearance kinetics in the joint, simultaneously rather than separately as done in the
341 previous studies[38] and furthers the ability to determine the relationship between lymphatic and
342 venous uptake *in vivo*.

343 Exercise has been shown in previous studies to increase interstitial[39], venous[40], and
344 lymphatic[41] flow to the muscle. In this study, we used exercise as an intervention to demonstrate
345 the sensitivity of multichromatic NIR imaging to measure changes to venous and lymphatic
346 clearance. In the joint space, exercise and joint loading have increased intra-articular pressure
347 and cartilage flux. In this study, we showed that injection that was followed by exercise
348 transiently increased lymphatic outflow from the joint; however, exercise did not have a
349 significant effect on venous clearance. Interestingly, running pre-injection led to delayed
350 clearance of both free dye and PEG, as exhibited by the presence of a larger peak intensity from
351 the joint than their respective controls, which could be a consequence of altered hydrodynamic
352 forces or delayed dye dispersion.

353 Our current setup limited our temporal sampling frequency in both in vivo experiments.
354 For running experiments, sampling frequency was limited by the time required for an animal to
355 recover from and back under anesthesia. An ideal setup would be a wearable sensor that would
356 go around the knee, which allows us to see the concentration in real-time without anesthesia.
357 Similarly, in capturing the routes of clearance in the tail, we could only use one channel at a time
358 due to our stereoscope's filter imaging limitations. Two cameras and light paths, or a
359 computerized filter wheel, would simultaneously assess these two tracers with higher temporal
360 frequency to quantify the relationship between vascular and lymphatic uptake *in vivo*.
361 Additionally, the tracer sizes were designed to evaluate the particulate transport within fluid;
362 however, there are also cell-mediated mechanisms by which transport occurs *in vivo,* which
363 could be imaged using these multichromatic approaches.

364 We conclude that multichromatic NIR imaging is capable of simultaneous imaging of
365 lymphatic and venous-mediated fluid clearance with great sensitivity and can be used to measure
366 transient changes in clearance rates and pathways. The fluorophores and materials could be
367 refined to provide more colors and construct sizes in the NIR range for 3 or 4 color imaging. The
368 NIR-II imaging window could be used to visualize deeper structures *in vivo.* This methodology

369 can be applied in future studies that assess the effects of diseases or surgical interventions on
370 interstitial solute transport and tissue fluid homeostasis.
371
372 **Figure Captions**
373 **Figure 1: *In vivo* NIR imaging methods**
374 **a.** Mouse tail injection and imaging methods. **b.** Intra-articular injections for assessing the effect
375 of exercise.
376
377 **Figure 2: Sensitivity Analysis of Near-Infrared Dyes with Tissue Phantoms**
378 **a.** Absorbance spectra show a unique absorption profile for each tracer. **b.** Solid and dashed lines
379 show the excitation/emission spectra for 800CW carboxylate (free dye) and 680RD 40 kDa PEG
380 (PEG), respectively. Our NIR stereoscope filter cube setup is represented by the bars above the
381 graph, showing that our optical configuration is designed to read each tracer's unique signal. **c.**
382 Tissue phantoms used to determine the effect of tissue depth on detecting free dye and PEG
383 showed reduced intensity as a function of phantom depth and serial two-fold dilution.
384 Consequentially, we were able to see a reduction in signal intensity below the background
385 (dotted line) and, therefore, could reach the limit for these tracers at this tracer at 25 ms exposure
386 and 100 ms exposure time respectively, using a 4 mm tissue phantom. **d.** Free dye was serially
387 diluted using a stock solution of PEG and vice versa. There was no change in overall intensity
388 and sensitivity for each tracer due to mixing and imaging in a 2 mm phantom.
389
390 **Figure 3: Co-injection of NIR tracers results in differential uptake of 800 CW Carboxylate**
391 **and 680RD PEG 40 kDa**
392 **a.** Evans blue dye injected into the tail of a mouse immediately before euthanasia shows the
393 concentration of Evans blue dye in the lymphatics (blue arrows) that flank the blood vessels (red
394 arrows) (scale bar = 1000 um). **b.** Free dye and PEG show the uptake of each NIR tracer in vein
395 and lymphatics 10 minutes post injection (scale bar = 1000um). **c.** Free dye can initially be seen
396 in the lymphatic; however, over time free dye concentrates in the circulation revealing the tail
397 vein. PEG shows the sustained uptake of PEG dye into lymphatics. **d.** Measurement of signal
398 intensity over the course of the four imaging windows for each respective tracer shows large
399 phasic lymphatic contractions for the PEG tracer and increasing free dye signal over time.

Figure 4: Co-injection of NIR tracers allows for the simultaneous detection of lymphatic and vascular mediated clearance from the joint space.
a. Clearance profiles for PEG and free dye show the characteristic lymphatic and venous clearance, respectively. **b.** The areas under the curves show a significantly lower AUC for free dye compared to the PEG. **c.** First-order clearance constant tau was calculated for each tracer and is significantly higher for the lymphatic draining PEG vs the venous draining free dye.

Figure 5: Clearance Profiles for PEG and free dye with running.
a-c. Clearance profile of lymphatic specific tracer (PEG) for no running, pre-injection running and post-injection running experiments. **d-f.** Clearance profile for venous draining (free dye) for No running, pre-injection running, and post-injection running experiments.

Figure 6: Effect of running on Normalized Change in Intensity and Normalized Tau
a, b. The normalized intensity was calculated to assess the transient effect of running on dye dispersion in the joint. For each experiment, all runners were normalized to the mean of non-running controls. Compared to the control experiment running pre- or post-injection did not significantly change the initial free dye intensity; however, at the second captured timepoint, post-injection normalized intensity was significantly decreased compared to pre-injection running (*, $p = 0.04$). After 1 hour, lymphatic intensity was significantly decreased compared to controls (*, $p = 0.01$) and pre-injection running (***, $p = 0.0003$) **c, d.** Time constant (tau) for each condition was normalized to the controls for each day. Compared to intraexperimental non-running controls, there are no significant differences in clearance rate for either tracer. Compared to running pre-injection, clearance rate is significantly decreased (*, $p = 0.04$).

Supplementary Video 1: Lymphatic uptake of PEG in mouse tail in four discontinuous imaging windows post-intradermal injection.

Supplementary Video 2: Venous uptake/concentration of free dye over four discontinuous imaging windows post intradermal injection.

428 **Supplementary Video 3:** Superimposed videos of lymphatic and venous uptake of PEG and free
429 dye in the mouse tail.

430

431 **References**

432 1. Hemant, S. Physiologic upper limits of pore size of different blood capillary types and
433 another perspective on the dual pore theory of microvascular permeability. *J. Angiogenes.*
434 *Res.* **2**, 1–19 (2010).
435 2. Pappenheimer, J. R., Renkin, E. M. & Borrero, L. M. Filtration, Diffusion and Molecular
436 Sieving Through Peripheral Capillary Membranes. *Am. J. Physiol. Content* **167**, 13–46
437 (1951).
438 3. Olszewski, W. L. The lymphatic system in body homeostasis: physiological conditions.
439 *Lymphat. Res. Biol.* **1**, (2003).
440 4. Zhao, J., Salmon, H. & Sarntinoranont, M. Effect of heterogeneous vasculature on
441 interstitial transport within a solid tumor. *Microvasc. Res.* **73**, 224–236 (2007).
442 5. Bouta, E. M. *et al.* The role of the lymphatic system in inflammatory-erosive arthritis.
443 *Semin. Cell Dev. Biol.* **38**, 90–97 (2015).
444 6. Frush, D. P. & Applegate, K. Computed tomography and radiation: Understanding the
445 issues. *J. Am. Coll. Radiol.* **1**, 113–119 (2004).
446 7. Goodman, T. R. Understanding the Cancer-CT Conundrum. **44**, 469–474 (2010).
447 8. Kim, S. J. & Kim, K. A. Safety issues and updates under MR environments. *Eur. J.*
448 *Radiol.* **89**, 7–13 (2017).
449 9. Moreno, M. J., Ling, B. & Stanimirovic, D. B. In vivo near-infrared fluorescent optical
450 imaging for CNS drug discovery. *Expert Opin. Drug Discov.* **15**, 903–915 (2020).
451 10. Tian, Y., Qiang, S. & Wang, L. Gold Nanomaterials for Imaging-Guided Near-Infrared in
452 vivo Cancer Therapy. *Front. Bioeng. Biotechnol.* **7**, (2019).
453 11. Zeng, H. C., Hu, J. L., Bai, J. W. & Zhang, G. J. Detection of Sentinel Lymph Nodes with
454 Near-Infrared Imaging in Malignancies. *Mol. Imaging Biol.* **21**, 219–227 (2019).
455 12. Stolik, S., Delgado, J. A., Pérez, A. & Anasagasti, L. Measurement of the penetration
456 depths of red and near infrared light in human ″ex vivo″ tissues. *J. Photochem. Photobiol.*
457 *B Biol.* **57**, 90–93 (2000).

458 13. Ash, C., Dubec, M., Donne, K. & Bashford, T. Effect of wavelength and beam width on
459 penetration in light-tissue interaction using computational methods. *Lasers Med. Sci.* **32**,
460 1909–1918 (2017).
461 14. Jagdeo, J. R., Adams, L. E., Brody, N. I. & Siegel, D. M. Transcranial Red and Near
462 Infrared Light Transmission in a Cadaveric Model. *PLoS One* **7**, 1–10 (2012).
463 15. Weiler, M., Kassis, T. & Dixon, J. B. Sensitivity analysis of near-infrared functional
464 lymphatic imaging. *J. Biomed. Opt.* **17**, 066019 (2012).
465 16. Weiler, M. & Dixon, J. B. Differential transport function of lymphatic vessels in the rat
466 tail model and the long-term effects of indocyanine green as assessed with near-infrared
467 imaging. *Front. Physiol.* **4 AUG**, 1–10 (2013).
468 17. Proulx, S. T. *et al.* Use of a PEG-conjugated bright near-infrared dye for functional
469 imaging of rerouting of tumor lymphatic drainage after sentinel lymph node metastasis.
470 *Biomaterials* **34**, 5128–5137 (2013).
471 18. Proulx, S. T., Ma, Q., Andina, D., Leroux, J.-C. & Detmar, M. Quantitative measurement
472 of lymphatic function in mice by noninvasive near-infrared imaging of a peripheral vein.
473 *JCI Insight* **2**, 1–13 (2017).
474 19. Kobayashi, H. *et al.* Simultaneous multicolor imaging of five different lymphatic basins
475 using quantum dots. *Nano Lett.* **7**, 1711–1716 (2007).
476 20. Mwangi, T. K. *et al.* Intra-articular clearance of labeled dextrans from naive and arthritic
477 rat knee joints. *J. Control. Release* **283**, 76–83 (2018).
478 21. Hama, Y., Koyama, Y., Urano, Y., Choyke, P. L. & Kobayashi, H. Simultaneous two-
479 color spectral fluorescence lymphangiography with near infrared quantum dots to map
480 two lymphatic flows from the breast and the upper extremity. *Breast Cancer Res. Treat.*
481 **103**, 23–28 (2007).
482 22. Ruddell, A. *et al.* Dynamic contrast-enhanced magnetic resonance imaging of tumor-
483 induced lymph flow. *Neoplasia* **10**, 706–713 (2008).
484 23. Doan, T. N., Bernard, F. C., McKinney, J. M., Dixon, J. B. & Willett, N. J. Endothelin-1
485 inhibits size dependent lymphatic clearance of PEG-based conjugates after intra-articular
486 injection into the rat knee. *Acta Biomater.* **93**, 270–281 (2019).
487 24. Weiler, M. J., Cribb, M. T., Nepiyushchikh, Z., Nelson, T. S. & Dixon, J. B. A novel
488 mouse tail lymphedema model for observing lymphatic pump failure during lymphedema

489 development. *Sci. Rep.* **9**, 1–15 (2019).
490 25. Edelstein, A. D. *et al.* Advanced methods of microscope control using μManager software.
491 *J. Biol. Methods* **1**, 10 (2014).
492 26. Schindelin, J. *et al.* Fiji: An open-source platform for biological-image analysis. *Nat.*
493 *Methods* **9**, 676–682 (2012).
494 27. James, M. J., Cleland, L. G., Gaffney, R. D., Proudman, S. M. & Chatterton, B. E. Effect
495 of exercise on 99mTc-DTPA clearance from knees with effusions. *J. Rheumatol.* **21**, 501–
496 4 (1994).
497 28. Dulin, J. A. *et al.* Influence of exercise on the distribution of technetium Tc 99m
498 medronate following intra-articular injection in horses. *Am. J. Vet. Res.* **73**, 418–425
499 (2012).
500 29. Modi, S., Stanton, A. W. B., Mortimer, P. S. & Levick, J. R. Clinical Assessment of
501 Human Lymph Flow Using Removal Rate Constants of Interstitial Macromolecules: A
502 Critical Review of Lymphoscintigraphy. *Lymphat. Res. Biol.* **5**, 183–202 (2007).
503 30. Karlsen, T. V, McCormack, E., Mujic, M., Tenstad, O. & Wiig, H. Minimally invasive
504 quantification of lymph flow in mice and rats by imaging depot clearance of near-infrared
505 albumin. *Am. J. Physiol. Heart Circ. Physiol.* **302**, H391-401 (2012).
506 31. Wallis, W. J., Simkin, P. A., Nelp, W. B. & Foster, D. M. Intraarticular volume and
507 clearance in human synovial effusions. *Arthritis Rheum.* **28**, 441–9 (1985).
508 32. Carr, J. A. *et al.* Shortwave infrared fluorescence imaging with the clinically approved
509 near-infrared dye indocyanine green. *Proc. Natl. Acad. Sci. U. S. A.* **115**, 4465–4470
510 (2018).
511 33. Coleman, P. J., Scott, D., Mason, R. M. & Levick, J. R. Role of hyaluronan chain length
512 in buffering interstitial flow across synovium in rabbits. *J. Physiol.* **526**, 425–434 (2000).
513 34. Coleman, P. J., Scott, D., Ray, J., Mason, R. M. & Levick, J. R. Hyaluronan secretion into
514 the synovial cavity of rabbit knees and comparison with albumin turnover. *J. Physiol.* **503**,
515 645–656 (1997).
516 35. Simkin, P. A. & Bassett, J. E. Pathways of microvascular permeability in the synovium of
517 normal and diseased human knees. *J. Rheumatol.* **38**, 2635–42 (2011).
518 36. Hadler, N. M. Synovial fluids facilitate small solute diffusivity. *Ann. Rheum. Dis.* **39**,
519 580–585 (1980).

520 37. Kohlhof, H. *et al.* Single Molecule Microscopy Reveals an Increased Hyaluronan
521 Diffusion Rate in Synovial Fluid from Knees Affected by Osteoarthritis. *Sci. Rep.* **6**,
522 (2016).
523 38. Mwangi, T. K. *et al.* Intra-articular clearance of labeled dextrans from naive and arthritic
524 rat knee joints. *J. Control. Release* **283**, 76–83 (2018).
525 39. Schütze, H., Hildebrandt, W. & Stegemann, J. The interstitial fluid content in working
526 muscle modifies the cardiovascular response to exercise. *Eur. J. Appl. Physiol. Occup.*
527 *Physiol.* **62**, 332–6 (1991).
528 40. Joyner, M. J. & Casey, D. P. Regulation of increased blood flow (Hyperemia) to muscles
529 during exercise: A hierarchy of competing physiological needs. *Physiol. Rev.* **95**, 549–601
530 (2015).
531 41. Havas, E. *et al.* Lymph flow dynamics in exercising human skeletal muscle as detected by
532 scintography. *J. Physiol.* **504**, 233–239 (1997).
533

Figure 1

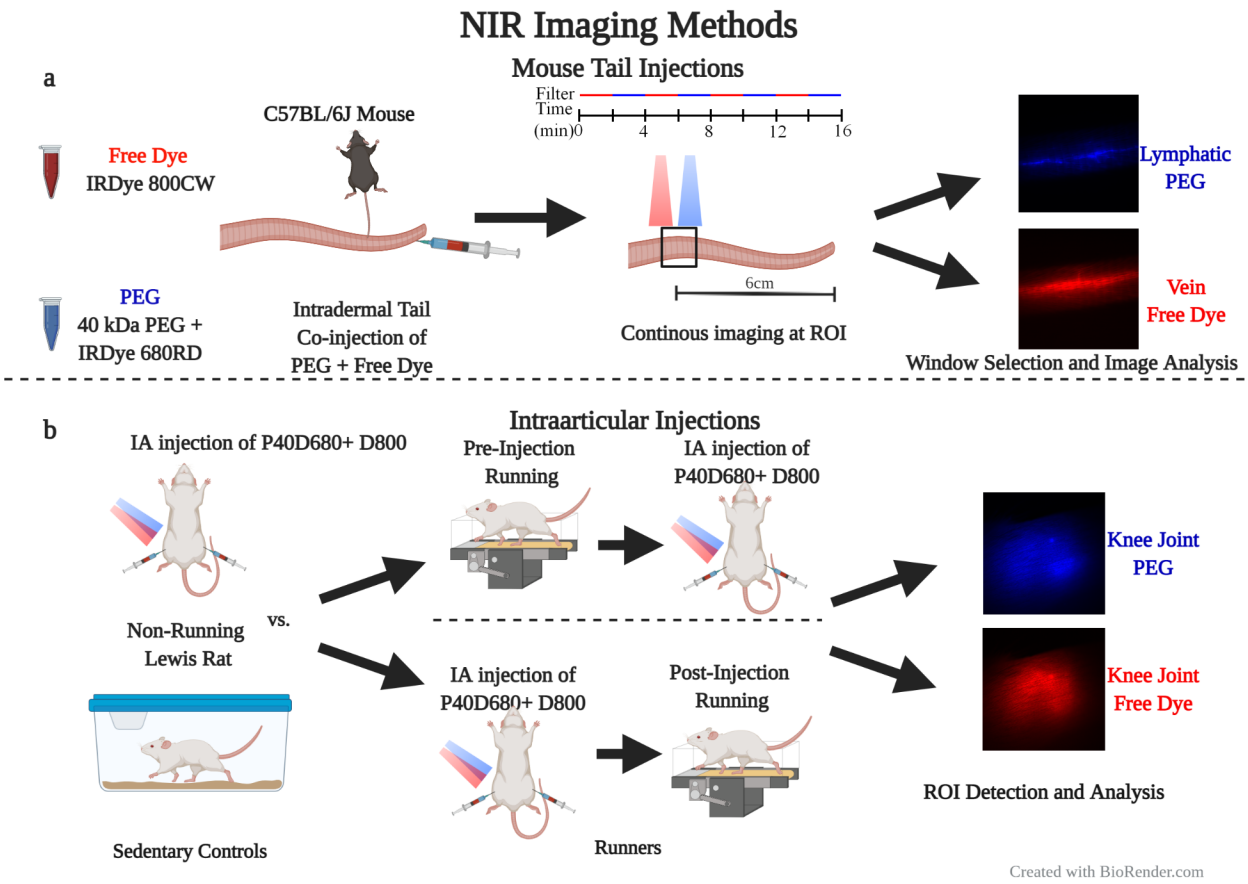
NIR Imaging Methods
a
Mouse Tail Injections
Free Dye
IRDye 800CW
C57BL/6J Mouse
Filter
Time
(min)0
4
8
12
16
Lymphatic
PEG
PEG
40 kDa PEG +
IRDye 680RD
Intradermal Tail
Co-injection of
PEG + Free Dye
6cm
Continous imaging at ROI
Vein
Free Dye
Window Selection and Image Analysis
b
Intraarticular Injections
IA injection of P40D680+ D800
Pre-Injection
Running
IA injection of
P40D680+ D800
Knee Joint
PEG
Non-Running
Lewis Rat
vs.
IA injection of
P40D680+ D800
Post-Injection
Running
Knee Joint
Free Dye
ROI Detection and Analysis
Sedentary Controls
Runners
Created with BioRender.com

Figure 2

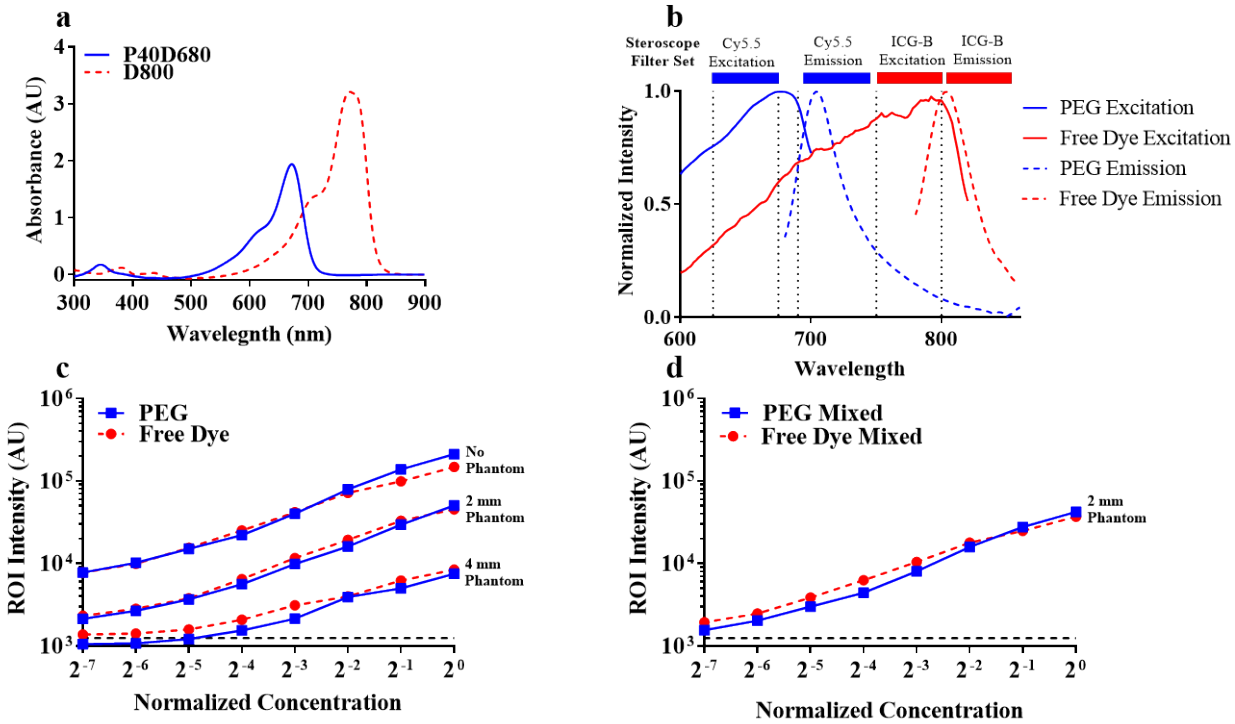
a
P40D680
D800
Absorbance (AU)
Wavelegnth (nm)
b
Steroscope Filter Set
Cy5.5 Excitation
Cy5.5 Emission
ICG-B Excitation
ICG-B Emission
Normalized Intensity
Wavelength
PEG Excitation
Free Dye Excitation
PEG Emission
Free Dye Emission
c
PEG
Free Dye
No Phantom
2 mm Phantom
4 mm Phantom
ROI Intensity (AU)
Normalized Concentration
d
PEG Mixed
Free Dye Mixed
2 mm Phantom
ROI Intensity (AU)
Normalized Concentration

Figure 3

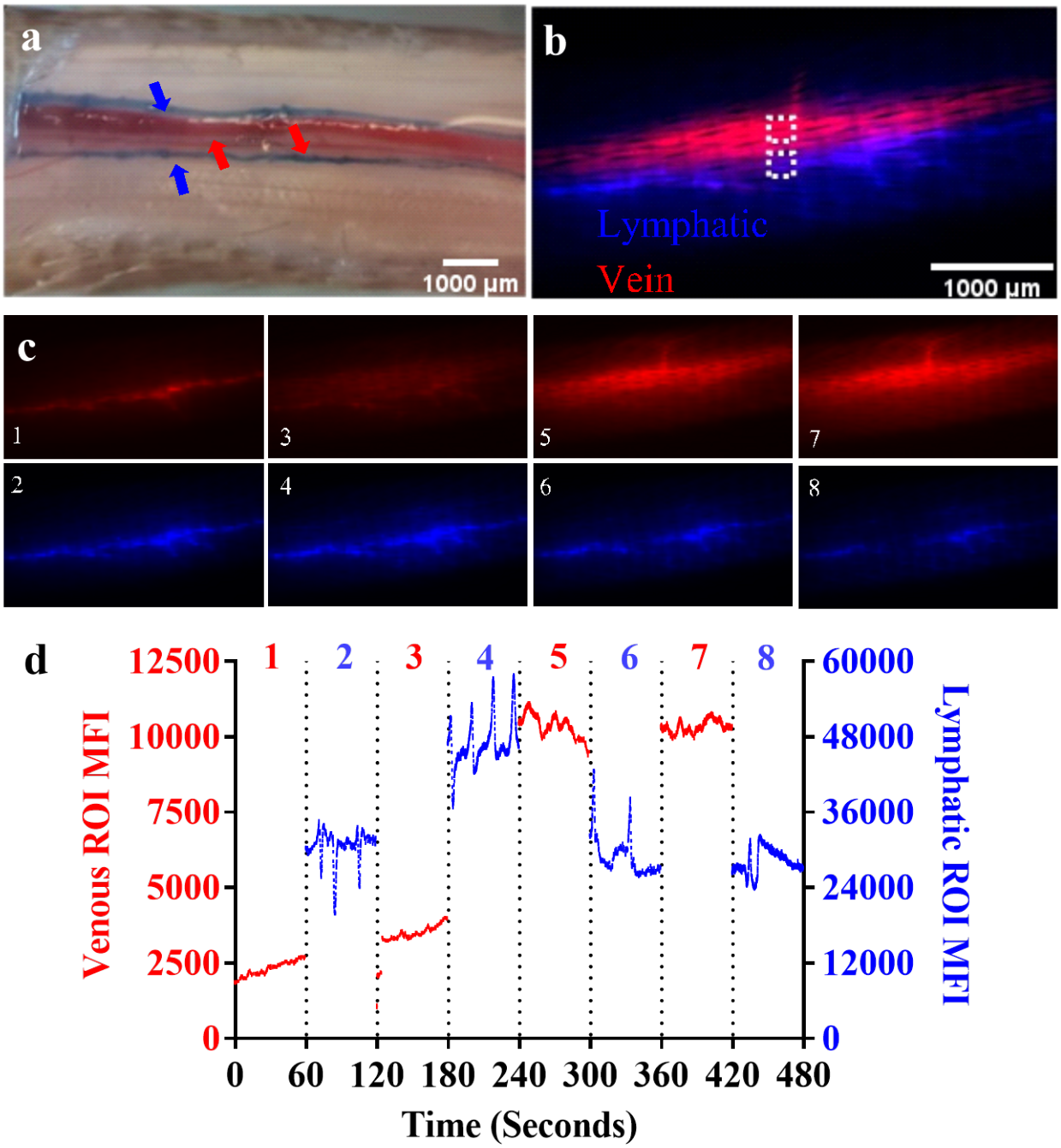
a
1000 µm
b
Lymphatic
Vein
1000 µm
c
1
3
5
7
2
4
6
8
d
Venous ROI MFI
12500
10000
7500
5000
2500
0
Lymphatic ROI MFI
60000
48000
36000
24000
12000
0
1
2
3
4
5
6
7
8
0
60
120
180
240
300
360
420
480
Time (Seconds)

Figure 4

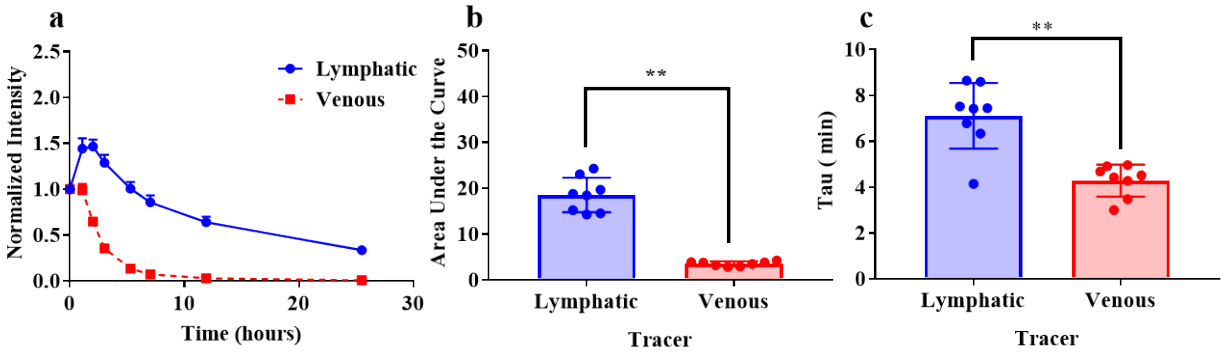
a
Normalized Intensity
2.5
2.0
1.5
1.0
0.5
0.0
0
10
20
30
Time (hours)
Lymphatic
Venous
b
Area Under the Curve
50
40
30
20
10
0
**
Lymphatic
Venous
Tracer
c
Tau (min)
10
8
6
4
2
0
**
Lymphatic
Venous
Tracer

Figure 5

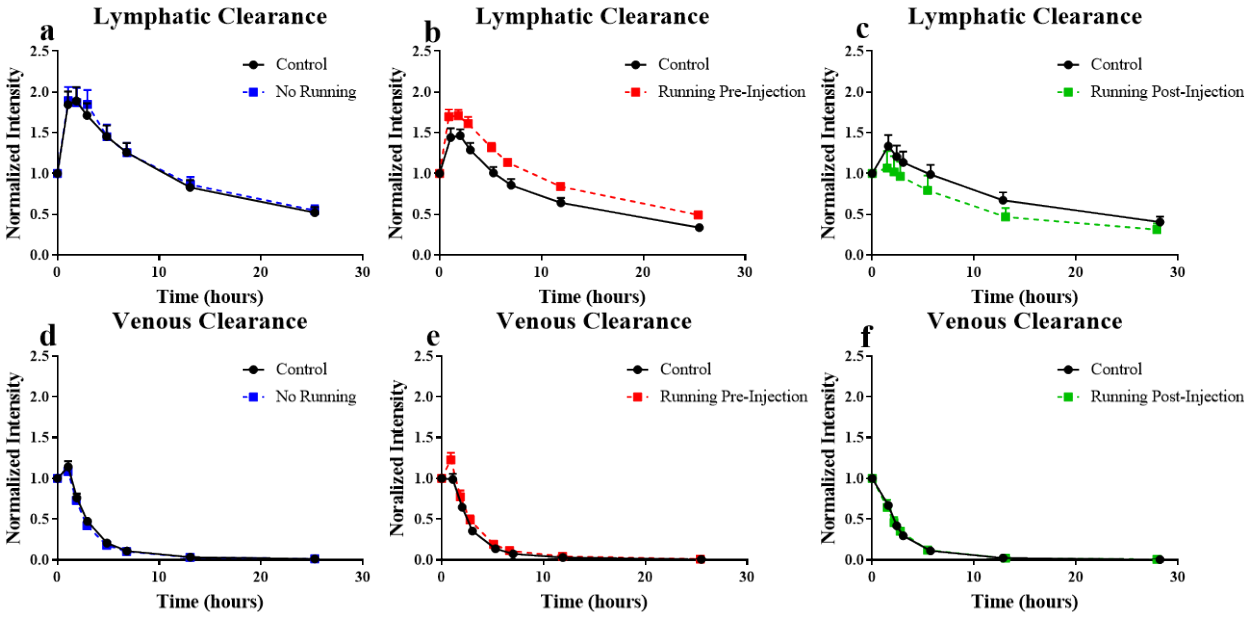
a
Lymphatic Clearance
Control
No Running
Normalized Intensity
Time (hours)
b
Lymphatic Clearance
Control
Running Pre-Injection
Normalized Intensity
Time (hours)
c
Lymphatic Clearance
Control
Running Post-Injection
Normalized Intensity
Time (hours)
d
Venous Clearance
Control
No Running
Normalized Intensity
Time (hours)
e
Venous Clearance
Control
Running Pre-Injection
Noralized Intensity
Time (hours)
f
Venous Clearance
Control
Running Post-Injection
Normalized Intensity
Time (hours)

Figure 6

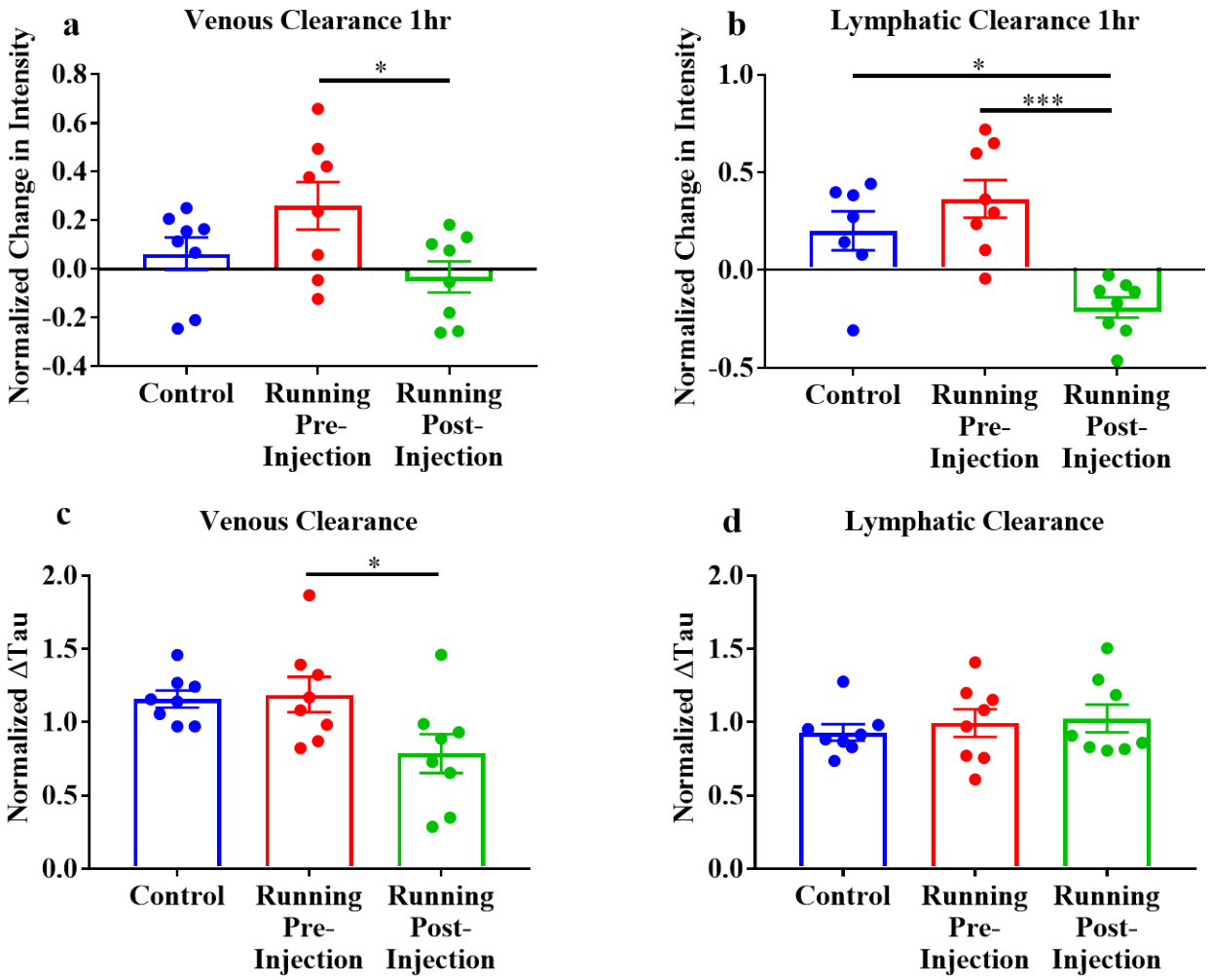
a
Venous Clearance 1hr
Normalized Change in Intensity
0.8
0.6
0.4
0.2
0.0
-0.2
-0.4
*
Control
Running Pre-Injection
Running Post-Injection
b
Lymphatic Clearance 1hr
Normalized Change in Intensity
1.0
0.5
0.0
-0.5
*
***
Control
Running Pre-Injection
Running Post-Injection
c
Venous Clearance
Normalized ΔTau
2.0
1.5
1.0
0.5
0.0
*
Control
Running Pre-Injection
Running Post-Injection
d
Lymphatic Clearance
Normalized ΔTau
2.0
1.5
1.0
0.5
0.0
Control
Running Pre-Injection
Running Post-Injection